Physical and chemical properties of sputter-deposited TaC_xN_y films

2006 J. Phys.: Condens. Matter 18 1977

(http://iopscience.iop.org/0953-8984/18/6/013)

INSTITUTE OF PHYSICS PUBLISHING JOURNAL OF PHYSICS: CONDENSED MATTER

J. Phys.: Condens. Matter **18** (2006) 1977–1986 doi:10.1088/0953-8984/18/6/013

Physical and chemical properties of sputter-deposited TaC_xN_y films

S M Aouadi[1,5], Y Zhang[1], P Basnyat[1], S Stadler[1], P Filip[2], M Williams[3], J N Hilfiker[4], N Singh[4] and J A Woollam[4]

[1] Department of Physics, Southern Illinois University, Carbondale, IL 62901-4401, USA
[2] Center for Advanced Friction Studies, Southern Illinois University, Carbondale, IL 62901-4343, USA
[3] Frederick Seitz Materials Research Laboratory, University of Illinois, Urbana, IL 61801, USA
[4] J A Woollam Co., Inc., 645 M Street, Suite 102, Lincoln, NE 68508, USA

E-mail: saouadi@physics.siu.edu

Received 20 October 2005
Published 25 January 2006
Online at stacks.iop.org/JPhysCM/18/1977

Abstract

The structural, electronic, optical, and mechanical properties of stoichiometric $TaC_xN_{y=1-x}$ were simulated using an *ab initio* calculation based on density functional theory (DFT) within the generalized gradient approximation. The calculations revealed the theoretical lattice parameter, density of states, refractive index, and elastic constants as a function of carbon and nitrogen content. TaC_xN_y films were subsequently produced on Si wafers using unbalanced magnetron sputtering. The structural, optical, and mechanical properties were measured using x-ray diffraction/transmission electron microscopy, vacuum ultraviolet spectroscopic ellipsometry, and nanoindentation, respectively. The computational and experimental properties were compared. The lattice parameter, the energy of the 2p bands in the density of states, and the energy of the interband transitions were found to decrease with increasing C content. No significant changes in the elastic constants were observed as a result of substituting N atoms with C atoms. The hardness and the elastic modulus were in the 40 and 380 GPa range, respectively. The experimental Young's modulus was much smaller than the computational one and this discrepancy was attributed to the nanocrystalline nature of the films. Also, the elastic constants were found to decrease dramatically for over-stoichiometric films.

(Some figures in this article are in colour only in the electronic version)

[5] Author to whom any correspondence should be addressed.

1. Introduction

Binary transition metal (TM) nitrides and carbides have been of great interest to the thin film community because of their superior mechanical properties, chemical inertness, electrical conductivity, and high melting point [1–3]. More recently, TM carbonitrides (TMCNs) were produced by various groups and were found to potentially have better properties than their binary counterparts. Some of the TMCNs that were reported in the literature include Ti–C–N [4–6], Cr–C–N [7, 8], Zr–C–N [9], and Ta–C–N [10].

This paper reports on an investigation of TaC_xN_y films deposited by reactive unbalanced magnetron sputtering. The TaC_xN_y films that were reported in the literature were fabricated as a potential diffusion barrier for copper metallization [10]. The main result of the study was that the thermal stability and chemical inertness of TaC_xN_y was superior to that of TaN or TaC. Moreover, the mechanical properties of binary TaC and TaN are outstanding due to their high hardness, which is a result of the covalent nature of their bonds [11]. Therefore, TaC_xN_y is a potential material for applications that require superior hardness in tandem with thermal and/or chemical stability. A systematic study of the thermochemistry of TaC_xN_y was carried out by Frisk [12] and included a calculation of the equilibrium phase diagram for these structures. She reported that, since TaN and TaC have similar crystal structure and electronic properties, they are miscible. In addition, non-stoichiometric materials may form other phases including multi-phase structures, and these phases include amorphous carbon (a-C) and Ta_2CN. The preparation method utilized in producing our films, i.e., sputtering, is known to produce metastable phases and, hence, the equilibrium phase diagram reported by Frisk [12] will be utilized as a reference.

The current study is divided into two sections. The first section reports on *ab initio* density functional theory calculations that were performed to investigate the effect of alloying with C on the structural, chemical, optical, and mechanical properties of TaN. The results obtained from the simulations represent the ideal case that corresponds to a crystalline single-phase $TaC_xN_{y=1-x}$ structure. The second part of the article deals with the fabrication and analysis of such films. Single-layer coatings of TaC_xN_y were deposited by unbalanced magnetron sputtering on Si(111) wafers. The following techniques were used to characterize these coatings: x-ray diffraction (XRD), transmission electron microscopy (TEM), Rutherford backscattering (RBS), x-ray photoelectron spectroscopy (XPS), vacuum ultraviolet spectroscopic ellipsometry (VUV-SE), and nanoindentation to analyse crystallographic structure, film architecture, elemental and phase composition, optical/transport properties, and hardness/elastic modulus, respectively. The experimental data are compared to the simulated ideal data. The effect of deviations from the ideal crystalline and stoichiometric structures results in differences between the computational and experimental quantities. A comparative study will help explain the effect of the extrinsic (non-ideal) properties of the films on their optical and mechanical properties.

2. Computational method

The ground state energies, lattice parameter, optical response, elastic constants, and electronic structure of $TaC_xN_{y=1-x}$ were calculated within the density functional theory (DFT) [13] formalism using the Cambridge Sequential Total Energy Package (CASTEP) software [14–16]. CASTEP uses a total energy plane-wave pseudo-potential method. In the mathematical model of the material, CASTEP replaces ionic potentials with effective potentials acting only on the valence electrons in the system. The electronic wavefunctions were expanded with a

Table 1. Deposition conditions for Ta–C–N films.

Sample	P_C (W)	P_{Ta} (W)	PP_{Ar} (Pa)	PP_{N2} (Pa)
S1	40	100	0.2	0.06
S2	70	10	0.2	0–0
S3	70	25	0.2	0.06
S4	70	40	0.2	0.09
S5	70	10	0.2	0.15
S6	35	10	0.2	0.15
S7	0	100	0.2	0.06

plane-wave basis set-up to a plane-wave cut-off energy sufficient for convergence, which varies depending on the convergence of each pseudo-potential. The electronic energies were mapped to a set of special k-points in the reduced Brillouin zone and the number of k-points was determined by the spacing in the reciprocal space. The exchange–correlation functional used in this study was the gradient corrected local density approximation of Perdew and Wang, or GGA-PW91 [17]. In order to achieve a high level of convergence of the total energy, a high-energy cut-off was chosen. The plane-wave cut-off was 340 eV. The total self-consistent field (SCF) energy change was 5×10^{-6} eV/atom and the energy between optimization steps was 5×10^{-5} eV/atom. An eight-atom cubic unit cell model with the rock salt structure was used to calculate the lattice parameter, the density of states, the dielectric functions, and the elastic coefficients. In order to study the effect of alloying on the various properties of the films, one or more N atoms were replaced by C atom(s) in the initial TaN structure.

3. Experimental procedure

TaC_xN_y films were deposited on Si(111) wafers using a dc reactive unbalanced magnetron sputtering system described in detail elsewhere [18]. The films were produced using individual Ta and C targets (99.99% purity) in a mixed Ar (99.999%) and N_2 (99.999%) discharge. Before deposition, the system was pumped down to 2×10^{-5} Pa using a turbomolecular pump backed by a rotary pump. The substrate, heated to 450 °C, was adjusted vertically to establish a substrate-to-target distance of 10 cm. Additionally, a radio frequency power supply was used apply a −100 V bias voltage to the substrate. The total thickness of the films, determined using the deposition rates deduced from analysing *in situ* spectroscopic ellipsometer data [18], was 2.0 μm. The deposition conditions that were varied are listed in table 1.

The crystallographic structure, the elemental composition, and the phase composition were determined using a GBC MMA (mini materials analyser) x-ray diffractometer (XRD) [19], a Rutherford backscattering system [20], and a Leybold Max200 x-ray photoelectron spectroscopy (XPS) apparatus [18], respectively. The structure of the films was also analysed using a Jeol 2010F field-emission analytic TEM/STEM operated at 200 kV [18]. The optical properties of the films were evaluated using a Woollam Co. VUV-VASE^{TM} variable angle spectroscopic ellipsometer for the vacuum ultraviolet in the spectral ranging from 130–1700 nm [21]. Film hardness was measured using a computer-controlled MTS Systems Corporation Nanoindenter XP nanomechanical testing system by incrementing the load up to a depth of 100 nm [18]. Hardness and elastic modulus were determined from the indentation depth of the unloading curve. To eliminate any influence of the substrate material on the measurement of Young's modulus, the penetration range of the indenter was limited to a depth $<0.1d$, where d is the film thickness.

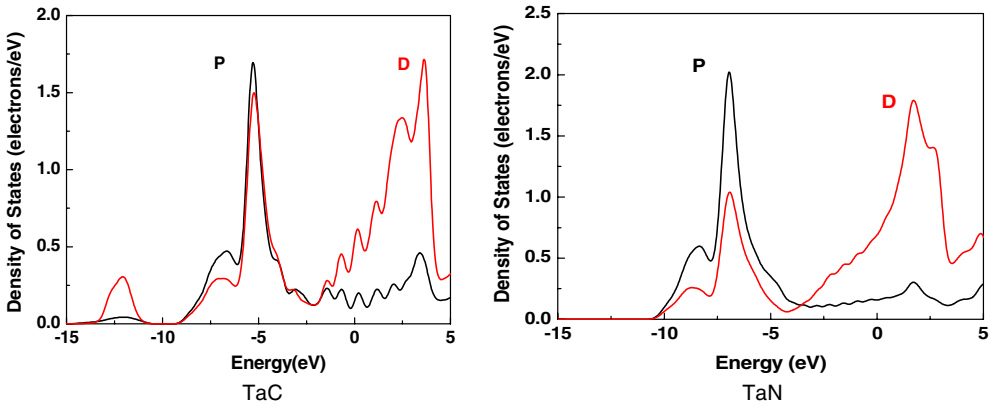

Figure 1. Calculated density of states for Ta–C–N.

Table 2. Calculated lattice parameters and lattice constants for Ta–C–N.

Sample	a (nm)	B (GPa)	E (GPa)	G (GPa)
TaC	0.442 952	359.73	730.48	230.88
$TaC_{0.75}N_{0.25}$	0.442 017	364.83	785.16	237.60
$TaC_{0.5}N_{0.5}$	0.441 292	363.41	735.51	193.34
$TaC_{0.25}N_{0.75}$	0.440 572	371.35	703.67	182.16
TaN	0.440 134	367.43	772.72	168.54
$TaC_{0.75}$	0.438 723	327.01	581.56	178.59
$Ta_{0.75}C$	0.436 340	284.30	631.44	195.41

4. Results and discussion

4.1. Computational analysis

The calculated total energies, E_{tot}, varied as a function of lattice parameter for the various $TaC_xN_{y=1-x}$ structures. Equilibrium lattice constants were determined from the minima of the curves and are shown in table 2. The lattice parameter was found to decrease when carbon was substituted for by nitrogen. Also shown in table 2 are the lattice parameters for non-stoichiometric TaC, which were found to be smaller than those that are stoichiometric.

Figure 1 shows the total density of states for TaN and TaC ($x = 0$ and 1). In this figure, the metal d orbitals of e_g symmetry hybridize strongly with the p states of nitrogen or carbon. The double-peaked structure found between -8 and -3 eV for TaN and between -10 and -5 eV for TaC originates from the non-metal 2p orbitals hybridizing with the metal d orbitals. This band was found to shift consistently between the values for TaN and TaC with x. The hybridization is strongest for the TaC system. These results are in agreement with the results obtained by Sahnoun *et al* [11] using the full-potential linearized augmented plane wave method. The shift in the 2p bands is caused by the additional valence electron from eight to nine for TaC and TaN, respectively. The intrinsic hardness and elastic modulus are therefore expected to be higher for TaC than for TaN as a result of the stronger hybridization and the more covalent nature of the bonds.

The calculated real and imaginary parts of the dielectric function for $TaC_xN_{y=1-x}$ films are shown in figure 2. This figure reveals peaks that correspond to electronic transitions between two states in different bands (interband transitions). Small peak shifts are predicted by the

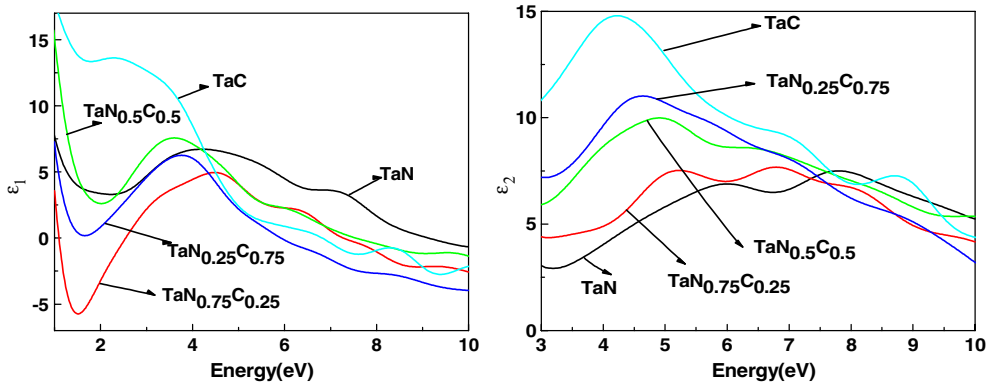

Figure 2. Calculated real and imaginary parts of the dielectric function for Ta–C–N.

simulation when N atoms are substituted for by C atoms (x varies between 0 and 1). These peak shifts may be correlated to the shifts in the DOS bands described earlier.

The theoretical behaviour of a completely asymmetric material is specified by 21 independent elastic constants, while for an isotropic material, there are two such constants. For a rock salt structure (cubic symmetry), there are three independent elastic constants, namely C_{11}, C_{44}, and C_{12}. The cubic symmetry was maintained for all substitutions of the N atoms with C atoms except when the number of substitution is two ($x = 0.5$). In this case, the lattice was tetragonal. The bulk modulus, B, may be directly derived from the second derivative of the total energy, E_{tot}, as a function of an isotropic volume change. B can also be expressed as a linear combination of two elastic constants as follows:

$$B = \frac{C_{11} + 2C_{12}}{3}.$$

The determination of the stress–strain distribution in a polycrystalline aggregate with respect to an external load can be established by equating the uniform strain in the polycrystal to the external strain in the Voigt approximation [22]. Hence, the shear modulus G and Young's modulus E can be calculated from the following relations:

$$G = \frac{3C_{44} + C_{11} - C_{12}}{5}$$

$$E = \frac{9BG}{3B + G}.$$

For the lattice with tetragonal symmetry, the shear modulus was calculated using the following expression:

$$G = \tfrac{1}{15}(2C_{11} + C_{33} - C_{12} - 2C_{13} + 6C_{44} + 3C_{66}).$$

The elastic constants were computed using CASTEP and the B, G and E values were calculated from the above equations are shown in table 2. No significant changes in the elastic constants were found to result from substituting N atoms with C atoms. The shear modulus was the only quantity that was found to increase with the increase in C content. The shear modulus describes the resistance of a material to a shape change and it plays an important role in the elastic theory of dislocations. It is usually correlated to the hardness of the material. The intrinsic hardness is, therefore, expected to be higher for TaC. The contribution of the extrinsic component may not be computed using *ab initio* techniques (need to consider dislocation motion) and could lead to experimental results that may be different from the theoretical predictions.

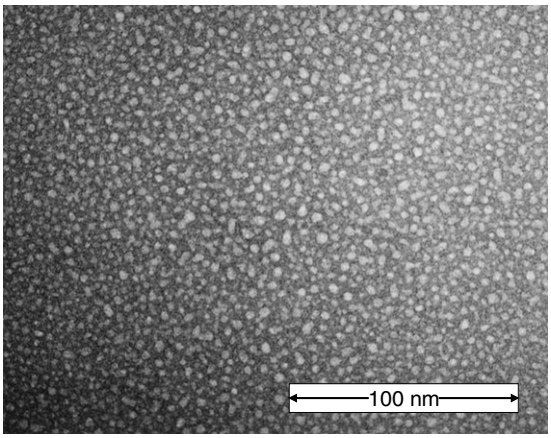

Figure 3. TEM micrograph for sample S1.

Table 3. Grain size and elemental and phase composition for Ta–C–N films.

Sample	*a* (nm)	Grain size (nm)	Ta (%)	C (%)	N (%)	Ta–C–N (%)	C–C (%)
S1	0.444 14	6.6	46	20	34	73	27
S2	0.447 50	13.5	53	47	0	62	38
S3	0.446 06	7.7	49	19	32	68	32
S4	0.437 37	27.5	45	26	29	68	32
S5	0.446 73	3.5	27	37	36	75	25
S6	0.448 23	20.0	36	39	25	49	51
S7	0.440 16	7.7	51	0	49	0	0

4.2. Structural analysis

X-ray diffraction patterns were recorded for the TaC_xN_y films. The diffraction patterns revealed multiple orientations of (111), (200), (220), and (311) Ta(C, N) crystal planes. The Ta(C, N) lattice belongs to the rock salt structure similar to that of TaN, with the interplanar spacing, *d*, becoming larger as more carbon atoms replace nitrogen atoms in the lattice. The crystallite sizes of the Ta(C, N) nanocrystals were determined using the Scherrer formula and are listed in table 3. Also presented in table 3 are the experimental lattice parameters, which were found to be comparable to the theoretical ones. The observed peak broadening for some of the samples may be the result of the grain refinement that may be the product of the formation of a nanocomposite structure [23]. For example, during the deposition of Ti–C films [24], a nanocomposite structure of the form nc-TiC/a-C (nanocrystals of TiC embedded in an amorphous C matrix) was produced. Similarly, nc-TiCN/a-C was produced during the deposition of Ti–C–N [4].

The representative plan-view TEM micrographs and selected area diffraction (SAD) pattern for sample S1 is shown in figure 3. These bright-field micrographs confirm that the films consist of a nanocomposite structure with nanometric dark grains of TaCN embedded in an amorphous matrix. The average grain size of the nanoparticles measured from the TEM micrographs was found to be consistent with the values deduced from XRD analysis (table 3).

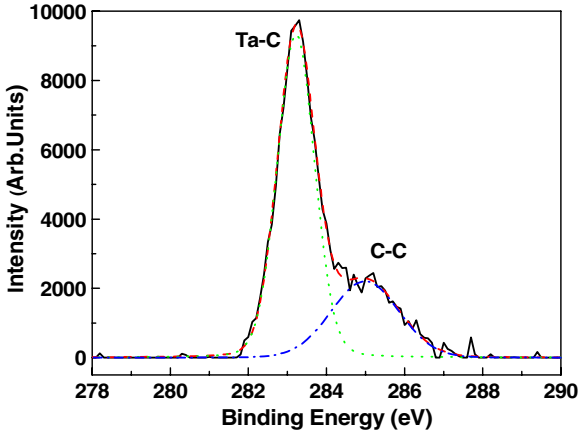

Figure 4. XPS spectra for S1 with an emphasis on C_{1s}.

4.3. Chemical analysis

RBS measurements were carried out to obtain the compositions, which were deduced from the simulation of the RBS data using the RUMP program (table 3). Interestingly, the films were nearly stoichiometric except for S5 and S6, which were excessively over-stoichiometric. High-resolution XPS spectra were recorded in order to evaluate the elemental and phase composition of the films. The atomic concentrations of the different elements were estimated using the areas under the C_{1s}, Ta_{4f} and N_{1s} peaks. This information is not shown since RBS provides more accurate results as it does not require sputter-etching of the surface [18, 20]. The spectra for Ta_{4f} and N_{1s}, not shown in this paper, consisted of peaks located at 23.3–23.5 eV and 398.0–398.7 eV, respectively. The data for both peaks agree well with what was previously reported for TaN [25]. A more detailed study of the C_{1s} peak was carried out to help elucidate the phase composition of these films. Figure 4 shows a typical C_{1s} spectrum which corresponds to that of S1. A representative curve-fitting of this spectrum is also included in this figure and it indicates the presence of two peaks that correspond to Ta–C (283.0–283.2 eV) and C–C (284.6–285.0 eV) [26]. The latter peak is attributed to a sp^2-coordinated bonds in graphite. The analysis of these spectra indicates that some of the carbon atoms replaced nitrogen in the TaN lattice to form a Ta(C, N) lattice, and other carbon atoms existed in an amorphous state in the grain boundaries. These findings are in agreement with the results obtained from analysing the TEM micrographs.

4.4. Optical analysis

The optical response of the films was measured using VUV-SE. Figure 5 shows the real and imaginary parts of the dielectric function with an emphasis on the interband transition region (from 3 to 9.5 eV). The calculated dielectric function is similar to the theoretical one (see figure 2) in that there is a shift in the interband transition(s) to higher energies when the composition is varied from that of TaC to TaN. The only spectra that do not follow this trend correspond to the over-stoichiometric samples, i.e. S5 and S6. These results could be reproduced theoretically by including vacancies in the calculations. Theoretical calculations predicted a shift in the Lorentz oscillator peak positions towards lower energies. For the other spectra, small differences between the calculated and experimental optical responses may

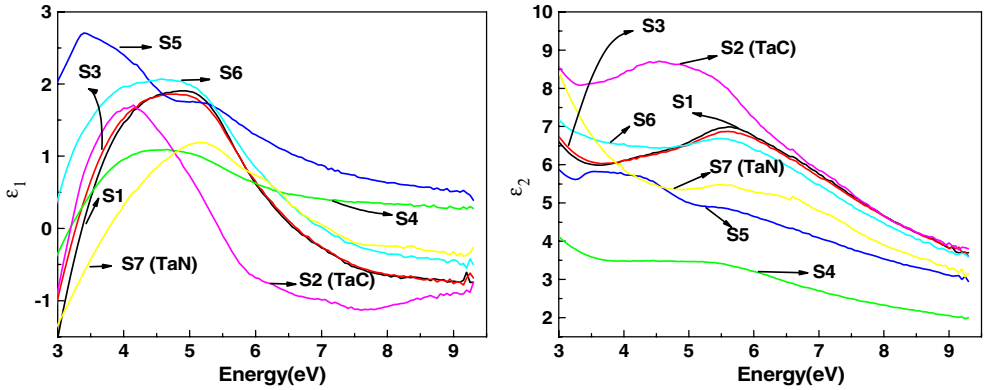

Figure 5. Measured real and imaginary parts of the dielectric function for Ta–C–N.

Table 4. Mechanical properties for Ta–C–N films.

Sample	E (GPa)	H (GPa)
S1	380 ± 30	36 ± 3
S2	350 ± 20	34 ± 3
S3	360 ± 20	33 ± 3
S4	380 ± 30	33 ± 3
S5	200 ± 30	18 ± 3
S6	260 ± 30	27 ± 3
S7	380 ± 30	42 ± 3

be noticed. One factor that contributes to this difference is the non-stoichiometric nature of some of our samples. Also, as expected, the experimental peaks are slightly broader than the simulated ones. The investigated compounds are vacancy-rich. Randomly distributed vacancies would smear out sharp peaks and thus contribute to the broadening in the measured data [20]. The nanocrystalline nature of the films is another major contributor to the observed experimental peak broadening due to the presence of different electronic wavefunctions at the grain boundaries [20].

The ellipsometric data were fitted using a single-layer model (since the films are optically thick) and the dielectric function of the Ta–C–N films was modelled as a superposition of a Drude term and one Lorentz oscillator [27]. The results of the simulation, not shown here, confirmed that the peak positions of the Lorentz oscillators shifted towards lower energies with increasing C content.

4.5. Mechanical analysis

Table 4 shows the hardness dependence of the TaC_xN_y films as a function of the various deposition conditions and elemental compositions that were investigated in the course of this work. The hardness was found to be in the 18–42 GPa range while the elastic modulus was found to vary between 200 and 380 GPa. These two quantities were found to depend on composition and microstructure. For samples with an elemental composition that is close to stoichiometry, the hardness was found to be in the 33–40 GPa range. The hardness was found to decrease dramatically for over-stoichiometric films. The theoretical and experimental elastic moduli results for stoichiometric films were in agreement in that they showed similar trends,

as shown in tables 2 and 4. A difference between the absolute values for E was expected since the deposited films were nanocrystalline and should exhibit a lower elastic modulus than the materials simulated using the *ab initio* method, which portray a crystalline material.

5. Conclusions

The structural, electronic, optical, and mechanical properties of ternary films of $TaC_xN_{y=1-x}$ were calculated using an *ab initio* approach based on DFT. TaC_xN_y films were subsequently produced by unbalanced magnetron sputtering and their structural, chemical, optical and mechanical properties were characterized using XRD/TEM, RBS/XPS, VUV-SE, and nanoindentation. The films were found to consist of nc-Ta–C–N/a-C (nanocrystals of Ta–C–N embedded in amorphous C matrix). The energy of the interband transition was found to decrease with increasing C content. The hardness of stoichiometric films was comparable to that of TaC or TaN. The hardness and the elastic modulus were in the 38 and 380 GPa range, respectively. However, the elastic constants were found to decrease dramatically for non-stoichiometric films.

Acknowledgments

The authors would like to thank Professor I Petrov and Dr R T Haasch for XPS measurements carried out in the Center for Microanalysis of Materials, University of Illinois, which is partially supported by the US Department of Energy under grant DEFG02-91-ER45439. This research was supported by an award from Research Corporation and by the Materials Technology Center and the Center for Advanced Friction Studies of Southern Illinois University (NSF grant EEC no 9523372).

References

[1] Amriou T, Bouhafs A, Aourag H, Khelifa B, Bresson S and Mathieu C 2003 *Physica* B **325** 46
[2] Holleck H 1990 *Surf. Coat. Technol.* **43/44** 245
[3] Sproul W D 1986 *Thin Solid Films* **107** 141
[4] Martinez-Martinez D, Sanchez-Lopez J C, Rojas T C, Fernamdez A, Eaton P and Belin M 2005 *Thin Solid Films* **472** 64
[5] Mani A, Aubert P, Khodja H and Houdy P 2003 *Mater. Res. Soc. Symp.* **778** 201
[6] Donnelly N, McConnell M, Dowling D P and O'Mahony J D 2000 *Mater. Sci. Forum* **325/326** 141
[7] Almer J, Odén M and Håkansson G 2001 *Thin Solid Films* **385** 190
[8] Čekada M, Maček M, Merl D K and Panjan P 2003 *Thin Solid Films* **433** 174
[9] Eerden M, Van Ijzendoom W, Tietema R and Van der Kolk G J 2003 *Annual Technical Conf. Proc. Society of Vacuum Coaters* p 56
[10] Wang S J, Tsai H Y, Sun S C and Shiao M H 2001 *J. Electron. Mater.* **30** 917
[11] Sahnoun M, Daul C, Driz M, Parlebas J C and Demangeat C 1998 *Comput. Mater. Sci.* **33** 175
[12] Frisk K 1998 *J. Alloys Compounds* **278** 216
[13] Dreizler R M and Gross E K U 1990 *Density Functional Theory* (Berlin: Springer)
[14] Milman V, Winkler V, White J A, Pickard C J, Payne M C, Akhmatskaya E V and Nobes R H 2000 *Int. Quantum Chem.* **77** 895
[15] Payne M C, Teter M P, Allan D C, Arias T A and Joannopoulos J D 1992 *Rev. Mod. Phys.* **64** 1045
[16] Segall M D, Lindan P J D, Probert M J, Pickard C J, Hasnip P J, Clark S J and Payne M C 2002 *J. Phys.: Condens. Matter* **14** 2717
[17] Wang Y and Perdew J P 1991 *Phys. Rev.* B **43** 8911
[18] Aouadi S M, Debessai M and Filip P 2004 *J. Vac. Sci. Technol.* B **22** 1134
[19] Khan M, Dubenko I, Stadler S and Ali N 2005 *J. Appl. Phys.* **97** 10M304

[20] Aouadi S M, Bohnhoff A, Amriou T, Haasch R T, Williams M and Hilfiker J N 2005 *J. Vac. Sci. Technol.* A **23** 705
[21] Hilfiker J N 2005 *Handbook of Ellipsometry* ed H G Tompkins and E A Irene (New York: William Andrew Publishing) chapter 12
[22] Mattessini M and Matar S F 2002 *Phys. Rev.* B **65** 075110
[23] Petrov I, Barna P B, Hultman L and Greene G E 2003 *J. Vac. Sci. Technol.* A **21** S117
[24] Stuber M, Leiste H, Ulrich S, Holleck H and Schild D 2002 *Surf. Coat. Technol.* **150** 218
[25] Aouadi S M and Debessai M 2004 *J. Vac. Sci. Technol.* A **22** 1975
[26] Dayan M, Shengli M and Xu K 2005 *Surf. Coat. Technol.* **200** 382
[27] Patsalas P and Logothetidis S 2001 *J. Appl. Phys.* **90** 4725